Turbulence structure around an asymmetric high-lift airfoil for different incidence angles.

I.Solís-Gallego*, A. Meana Fernández, J. M. Fernández Oro, K. M. Argüelles Díaz and S. Velarde-Suárez.

Fluids Mechanical Area, Departament of Energy

University of Oviedo

Edificio Departamental Este, Campus Universitario, 33203 Gijón, España (Spain)

*Corresponding author: *Phone: +0034 985 182661*, e-mail: *solisirene@uniovi.es*

Abstract

An exhaustive investigation of the structure of the turbulence around an asymmetric FX 63-137 wind turbine airfoil is carried out in this paper. Reliable hot-wire velocity measurements, made at the Xixon Aeroacoustic Wind Tunnel, are presented with the aim of analyzing the turbulent flow features. The probe was placed at two different positions along the streamwise direction, one over the airfoil and the other at the wake, both on the suction and pressure side. These measurements were performed in order to capture the evolution of the flow and its behavior at the wake. The experimental data were collected at a Reynolds number of 350000 for several incidence angles to explore their influence in the turbulence characteristics. The data processing from the dual hot-wire, capable of measuring two velocity components, allowed to achieve half set of the Reynolds stresses, the turbulence intensity and the degree of anisotropy. The boundary layer and wake size were estimated from the Reynolds stress components. In addition, the production term of the turbulence kinetic energy budget is calculated to visualize the unsteadiness energy inside the boundary layer. As a result of these analyses, it was observed that the transversal fluctuations were higher than the longitudinal ones. Besides, an alternative description of the turbulence structure is obtained when a frequency analysis of the motion is provided, disclosing a clear change in the spectra tendencies in the wake and boundary layer regions. This analysis, combined with the degree of anisotropy analysis, was helpful to define a transition zone between the clearly distinguishable instability zone and the free-stream zone. Finally, the integral length scale of turbulence was estimated from the area under the autocorrelation function of the velocity fluctuations. The combination of the results of this work have provided a wide description of the turbulent behavior of the flow around the airfoil and present a clearer physical picture of the phenomena.

Keywords: hot-wire anemometry; turbulence; wind turbine airfoil; wake; boundary layer; unsteadiness

NOMECLATURE

c	*Airfoil chord length, [m]*
Re	*Reynolds number, [-]*
α	*Flow incidence angle, [°]*
φ	*Total velocity and longitudinal velocity component angle, [°]*
x	*Streamwise cartesian coordinate, [m]*
y	*Wall-normal cartesian coordinate, [m]*
N	*Number of samples, [-]*
$L1$	*Wake position*
$L2$	*Airfoil position*
U_x	*Streamwise velocity component, [m/s]*
U_y	*Normal velocity component, [m/s]*
U_{max}	*Maximum velocity, [m/s]*
U	*Free-stream velocity, [m/s]*
$\overline{U}$	*Mean velocity, [m/s]*
u'	*Streamwise velocity fluctuation, [m/s]*
v'	*Normal velocity fluctuation, [m/s]*
w'	*Spanwise velocity fluctuation, [m/s]*
$Pk, total$	*Total production term, [m^2/s^3]*
$Pk, shear$	*Shear production term, [m^2/s^3]*
$Pk, curvature$	*Curvature production term, [m^2/s^3]*
U_Θ	*Polar coordinate of the mean velocity, [m/s]*
u_Θ'	*Polar coordinate of the mean longitudinal velocity fluctuation, [m/s]*
R_c	*Ratio of curvature of the airfoil,[m]*
TI	*Turbulence Intensity, [%]*
DA	*Degree of anisotropy, [-]*
PSD	*Power Spectra Density, [m/s^2Hz^{-1}]*
f	*Frequency, [Hz]*
ACF	*Autocorrelation function*
t	*Time, [s]*
τ	*Time lag, [s]*
ILS	*Integral Length Scale, [m]*

1. Introduction

The spatial and spectral distributions of turbulence parameters around an airfoil at different incidence angles, are of great interest in aircraft and turbomachinery structural studies. Specially, the study of boundary layers and wakes behind their blades and airfoils is crucial

to improve the performance of these machines. Particularly, drag reduction is one of the main factors to be considered for aerodynamic design, as it opposes to the relative motion of any object with respect to a surrounding fluid. Drag forces can be divided into friction drag, due to surface tangential stresses, and pressure drag, due to surface normal stresses (Kundu, et al., 2016). Because of the strong link between turbulence and friction drag as well as drag and energy consumption, there is a strong need to perform research in order to lower the overall drag. As a starting point to satisfy this necessity, a correct treatment and study of boundary layers and turbulent structures around airfoils are required.

The complex and random nature of the turbulence makes it a complicated phenomenon to study. The measurements of the turbulent fluctuating components themselves or of their mean values, is rather difficult and requires sophisticated equipment. As a consequence, much effort is invested in their understanding and the detailed work necessary to achieve a complete sight of the turbulence is still indispensable for practical application and research. The measurements of the mean values is quite sufficient for most practical applications, but only through the actual measurements of the fluctuating components it is possible to gain a deeper understanding of the mechanism of turbulent flow. In recent years, an increasing number of experimental investigations in turbomachinery have studied in detail the physical aspects of both turbulence and unsteady flow patterns (Velarde-Suarez, et al., 2002; Fernández Oro, et al., 2008; Yarusevych, et al., 2004). Total unsteadiness in multistage environment is a key parameter in the performance of any turbomachine. Therefore, Camp and Shin (1995) have processed turbulence data from a multistage compressor while Fernandez Oro et al. (2007) have analyzed the structure of the turbulence in a single stage low-speed axial fan. Alternatively, some authors focus on the study of the turbulence flow in other engines such as wind turbines. Moldano et al. (2015) and Farsimadan and Mokhtarzadeh-Dehghan (2010) performed different investigations of turbulence quantities in the boundary layer and near-wake of symmetric airfoils suitable for wind turbines at different angles of attack. The results highlighted the importance of achieving a good understanding of the boundary layer flow on the body from which the wake starts to develop. By changing the angle of attack of the airfoil with respect to the incoming flow, it was possible to modify the boundary layer development and thus study its effects on the wake.

The understanding of the flow around an airfoil is also the starting point for aeroacoustical studies. The type of boundary layer around the airfoil and its propagation to the wake are the main keys to identify qualitatively the noise source, particularly the airfoil self-noise (Brooks & Marcolini, 1986).

Several authors have investigated the mean-flow and turbulence characteristics around an airfoil as a former step to a better comprehension of the noise produced by itself (Kunze, 2004; Nakano, et al., 2006).

Their results show that the study of aerodynamic and turbulent flow parameters is a good procedure that leads to a better knowledge of the aerodynamic noise generation mechanisms in airfoils. According to Selig and McGranahan (2004), a set of the flow characteristics around a representative small wind turbine airfoil is a reliable and self-consistent database that should be helpful in validating aeroacoustics prediction codes in support of design activities.

In this paper, the results of a detailed experimental investigation of the unsteady flow around an airfoil at two positions in the streamwise direction are presented. Based on the measured velocity signals, the turbulent characteristics of the flow are determined. The influence of the angle of attack and the measurement position on the unsteadiness has been also analyzed. The experimental study of the turbulence at airfoil boundary layers and wakes at low Reynolds numbers has proved to be essential to improve the physical understanding of this complex phenomenon, in order to progress in the prediction techniques as well as design quieter and more efficient airfoils.

2. Experimental methodology

2.1 Experimental setup

A 1:1 scale FX 63-137 airfoil model was built with a span of L=1.1 m and a chord length of 0.305 m to carry out the hot-wire measurements. This airfoil was designed by F.X. Wortmann for the Liver Puffin human-powered aircraft. It has since been used for many low-Reynolds-number applications, especially in the small wind turbine area, because of its high-lift, soft-stall characteristics in addition to its overall good performance. The airfoil was carved out of a piece of aluminum on a numerically controlled machine. It is place in the test chamber of the Xixon Aeroacoustics Wind Tunnel, whose characterization had been previously made by Lastra et al. (2013) in a very descriptive way.

The wind tunnel is a closed loop circuit, arranged in a vertical layout (Fig. 1). The total length of the tunnel is 24.6 m, 8.3 m high and maximum operative velocities in the range of 22 m/s for the test section; i.e., a maximum Reynolds number of 1.7×10^6, based on the outlet hydraulic diameter of the nozzle (i.e., the outlet width).

Besides the characterization of the tunnel, other variables as the turbulence intensity were measured by Lastra et al. (2013) in order to know the tunnel flow quality, concluding that the turbulence intensity levels for the whole range of velocities available were found to be lower than 0.7 %.

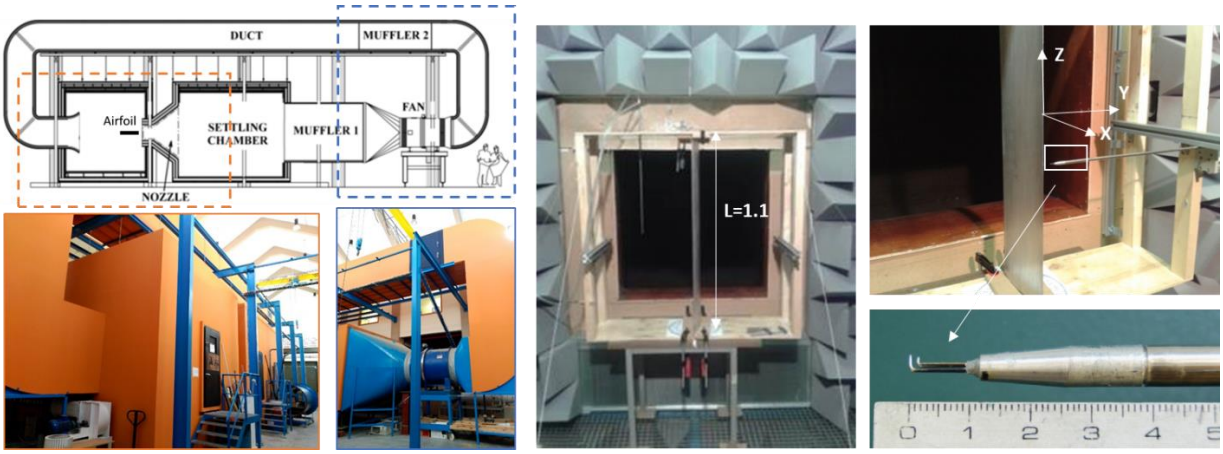

Fig. 1. Xixon Aeroacoustic Wind tunnel and assembly with a detail of the X-probe.

2.2 Dual hot-wire anemometry

The velocity distributions were measured with a home-made constant temperature X-wire probe, connected to a TSI IFA 100. Hot wire anemometry is a well-established, accurate and reliable technique to measure the flow velocity. The constant temperature anemometer works on the basis of convective heat transfer from a heated sensor to the surrounding fluid, being the heat transfer primarily related to the fluid velocity. By using very fine wire sensors (a typical wire is 1 mm length and 5 μm diameter) placed in the fluid and electronics with servo-loop technique, it is possible to measure velocity fluctuations of fine scales and of high frequencies.

Fig. 2 illustrates an outline of the procedure to collect the data and an example of the signal captured after transforming the data with the appropriate calibration. The IFA 100 outputs where connected to a National Instruments acquisition card that gave information to a computer. All the aspects of calibration of the probe, capture, record and conversion of measurements were driven by a MATLAB© code, particularly developed for this kind of applications. The uncertainty of absolute velocity has been estimated to be 0.75% in the center of the angular calibration range, while the angular uncertainty has been estimated to be 1° at the center of the measurement range. More details of the procedures and the uncertainty analysis of the probe are described in Blanco et al. (1998) and Fernández Oro et al. (2007a).

The analog voltage signal was first low-passed at 5 kHz using an analog filter to avoid aliasing. Then, it was sampled at 10 kHz over 25 s period through a data acquisition card, obtained a signal of $2.5x10^5$ samples per position. Converge study of the mean velocity data is made, checking that the sample data is high enough for the phenomena under study (Fig. 2).

The probe was placed at several positions in order to sweep the whole zone between the airfoil and the lateral wall of the test section. These sweeps were carried out in two positions along the streamwise direction: L1, which is located in the wake of the body, exactly at x= 1.108c from the leading edge and L2, which is located on the airfoil, at 75% of the chord, i.e. x=0.764c from the leading edge. These positions can be seen in Fig. 2 and in the following, Wake (L1) and Airfoil (L2) is used to refer them. This last position was chosen because it is a representative position of the high airfoil curvature. Measurements were made on both sides of the body: one on the suction side and another on the pressure side. Measurements were carried out for four incident angles, α = [-2.5°, 2.5°, 7.5°, 12.5°], and a $3.5x10^5$ Reynolds number. Fig. 1 shows the experimental setup placed at the test section inside the wind tunnel and the probe used in the hot-wire measurements.

3. Experimental results and discussion

The experimental data collected in this investigation are presented in the following manner. Firstly, the velocity measurements and turbulence intensity are studied to understand the basic flow parameters. Secondly, the Reynolds stress tensor components are obtained with respect to the variation of the incidence angle and the dimensions of the wake are presented. Then, the degree of anisotropy is calculated to find the directionality of the flow. Additionally, velocity spectra are analyzed to determine how the power of the signal in the time domain is distributed over the different frequencies and to visualize the instability zone. Finally, the integral length scale is estimated to identify the spatial dimension of the turbulence structure.

3.1 Velocity measurements and turbulence intensity

The measurements performed by the hot-wire probe, which is placed in the wind tunnel test chamber, can be used to characterize the turbulence generated by the airfoil. In this section, the streamwise velocity data and the angle between the total velocity and the longitudinal component of the flow, obtained directly from the hot-wire measurements, are presented. In addition, the streamwise turbulence intensity, which expresses the "strength" of the turbulent motion, was calculated. It is defined as:

$$TI = \frac{\sqrt{\overline{u'^2}}}{\bar{U}} 100 \quad (1)$$

where the over bar denotes the time-averaging value, U is the instantaneous velocity at the location of the hot-wire probe, and the $\overline{u'^2}$ represents the mean random fluctuations to the square.

A. Wake

Firstly, the velocity components at L1 for different values of the incidence angle (α) are analyzed by sweeping a line along the normal direction. The velocities have been made dimensionless with the maximum velocity of the collected data. To achieve a better visualization of the wake, the data were aligned relatively to the wake center and not to the trailing edge to place the minimum local velocity at y/c=0 (Fig. 3).

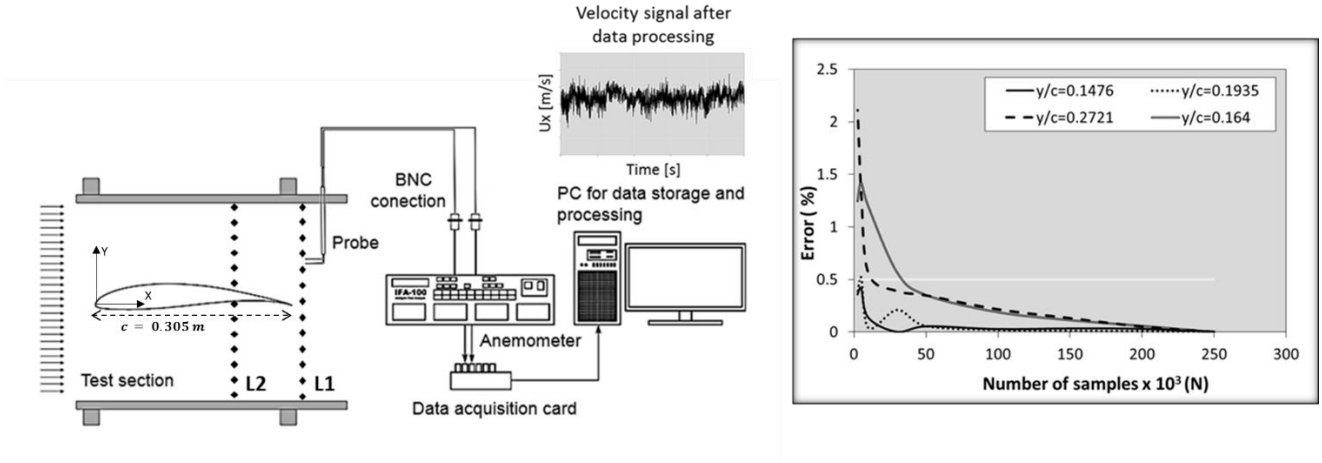

Fig. 2. Measurement chain and convergence study of mean velocities for four particular position.

Whenever the angle is modified, the velocity distributions are altered, causing changes in the main characteristics of the wake. These changes are shown in Fig. 3 as a shadow area which increases gradually from the smallest to the highest incidence angle. Besides modifications in the wake width and depth, an asymmetry in the shape of the wake was deduced from the results. Apart from the modification of the incidence, one of the causes of wake asymmetry is the airfoil loading, related to the asymmetric high-lift airfoil geometry. This loading has a substantial effect not only on the velocity profile but also on the turbulence structure, which is further explained in Section 3.2, where Reynolds stress components are analyzed. As above mentioned, these velocity measurements were realized with an uncertainty of 0.75%.

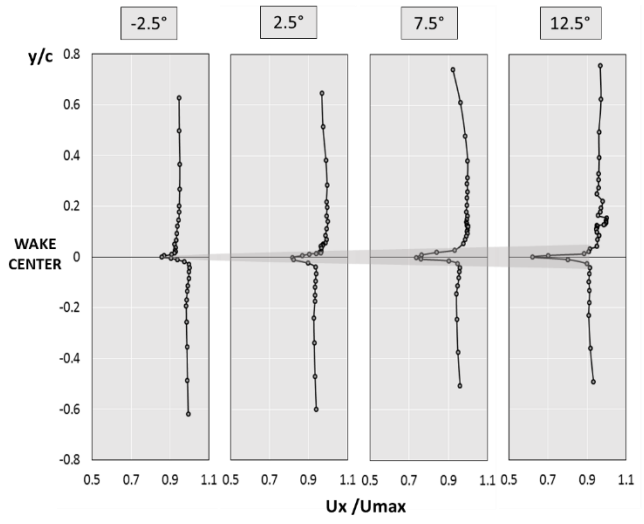

Fig. 3. Longitudinal velocity component measurements in the wake for different angles of attack.

Hah and Lakshminarayana (1982) reported an experimental investigation of the turbulence characteristics in the near wake of an airfoil, which also showed an asymmetrical behavior according to the incidence angle variations. Moreover, Liu (2001) focused on a wake shape basic research, in which a systematic investigation into the response of symmetric and asymmetric planar turbulent wake development to constant adverse, zero and favorable pressure gradients was conducted, concluding that the asymmetric wake widens much faster than the symmetric wake and produces a higher velocity defect compared with the symmetric ones. Other characteristic of the wake is its different behavior depending on the airfoil side. On the suction side, the velocity is higher than on the pressure side, except for the negative angle in which the opposite effect arises. On the other hand, the center of the wake in the vicinity of the trailing edge is shifted to the pressure side along the normal direction as the angle of attack increases. This effect is depicted in Fig. 4, where the wakes have not been aligned with y/c=0. As a last contribution, as the measurements move away from the instability area, the flow becomes uniform, reaching the free-stream velocity flow, and then keeps constant.

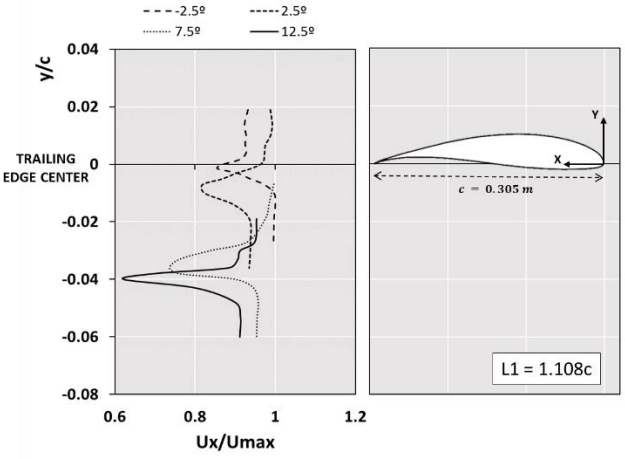

Fig. 4.

In Fig. 4, the absolute angle between the total velocity and longitudinal component is shown. In general, the angle does not exceed 20° and the biggest variations in the values are presented in the highest angle with an angular uncertainty of 1°.

Concurrently, the streamwise turbulence intensity at the wake was calculated. A contour map, with a zoom in the normal axis to achieve a more visible graph, is plotted in Fig. 5. The wake centerline refers to the localization of the minimum velocity in the wake corresponding with y/c=0. The maximum values of the turbulence intensity appear for the highest incidence angle, reaching a value of 14%. It should be pointed out that this maximum is found on the suction side of the wake, i.e. positive values from the wake centerline. The contour map agrees with the stream velocity measurements, showing that the area where the turbulence intensity is higher is in concordance with the wake dimensions, which increase with the angle of attack. As it is expected the highest turbulence levels are for the 12.5° angle that

presents the greatest wake dimensions, as shown visibly Fig. 3. The negative incidence angle presents more turbulence intensity on the pressure side (5%) than on the suction side (4%), while for positive angles the high turbulence intensity is shown on the suction side. This is owing to the fact that for negative angles the pressure side behaves as the suction side for positive angles.

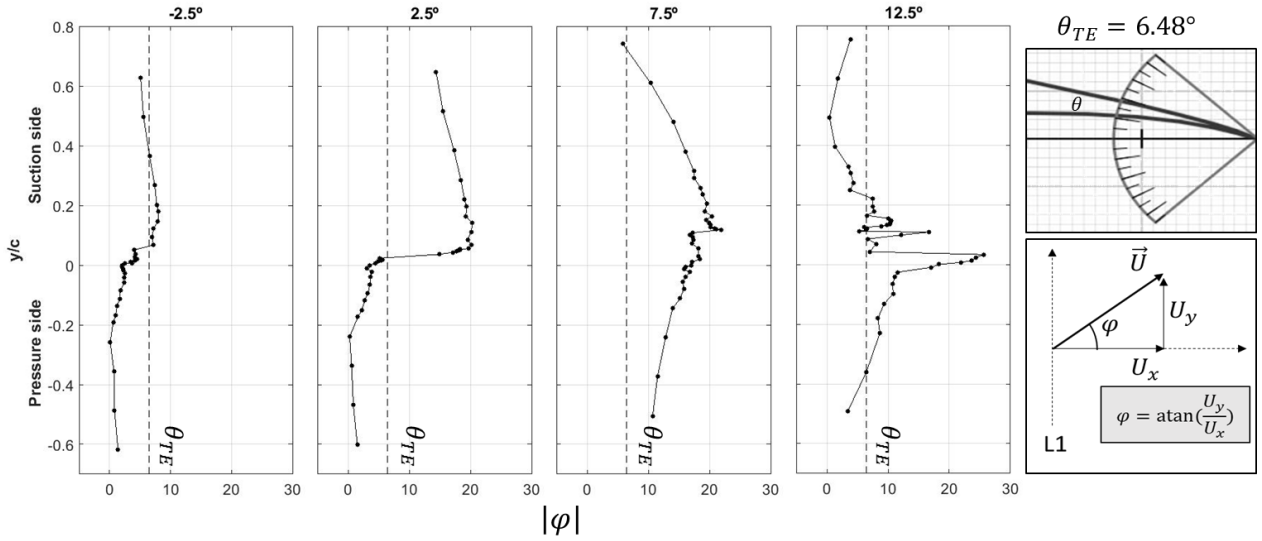

Fig. 5. Angle between the total velocity and the longitudinal component of the flow in the wake for different angles of attack.

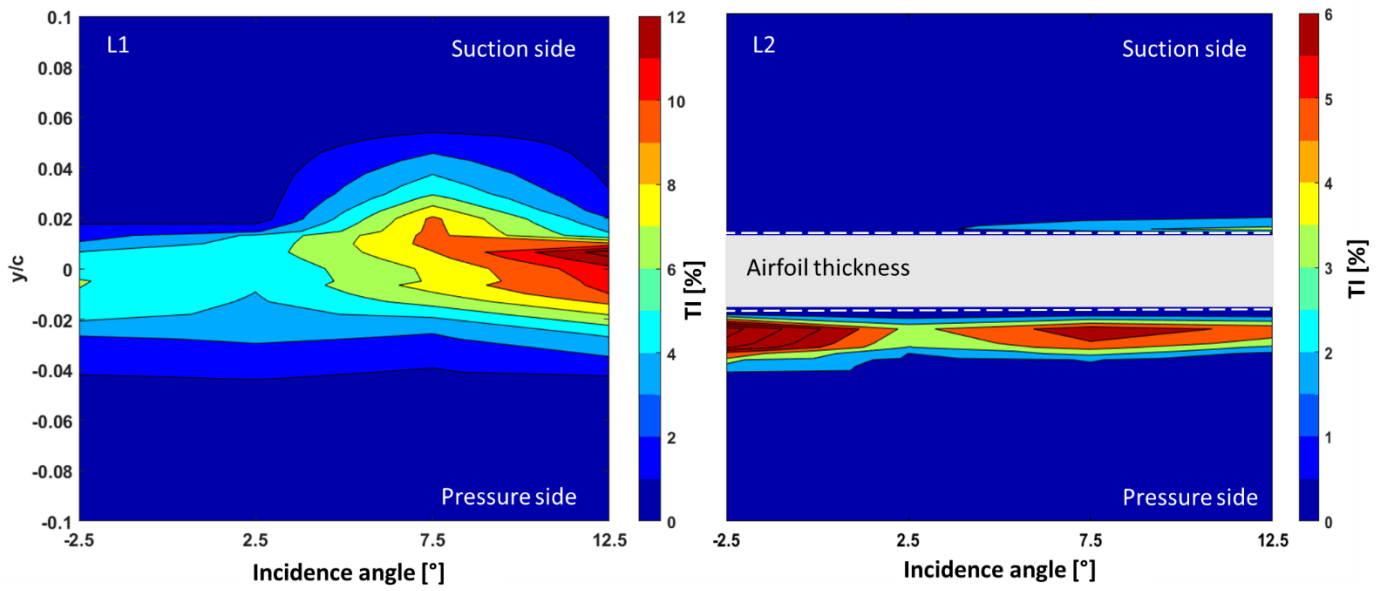

Fig. 6. Contour map of turbulence intensity at L1 and L2 position.

B. Airfoil

As in subsection A, Fig. 6 illustrates the streamwise velocity component and the angle between the total velocity and its longitudinal component at 75% of the airfoil chord, which corresponds to the L2 position, with an absolute velocity uncertainty of 0.75% as well as an angular uncertainty of 1°. The same behavior is shown for both variables, presenting the highest values on the suction side of the airfoil. Figure 6 shows typical velocity profiles with a steep increase near the wall and a fairly uniform velocity center-line. In the velocity graphs, the boundary layer on the pressure side seems to decrease drastically, while on the suction side this behavior only appears for the highest angle (12.5°). The suction side velocities increase until reaching a maximum, but the values do not decrease as for the 12.5° angle because the boundary layer is very thin, even for 7.5°. This behavior is explained in the following sections in detail. It can be seen that for the negative incidence angle the contrast between suction and pressure side velocities is lower than for the positive angles. However, in the velocity angle figure (Fig. 6, right side), the opposite behavior is shown, with the contrast between airfoil sides higher for positive angles. In general, the velocity angle is small, being the 12.5° angle the one which presents the greatest value (35°). Finally, it has been noticed that the pressure face data are less uniform than the suction face data, and the angle values near the wall increase, tendency that opposes to the velocity graph tendency, where the values in this zone decrease.

On the suction side of this position (L2), the turbulence intensity could not be correctly estimated due to the impossibility of capturing enough values from the thin boundary layer. In order to protect the probe, it is not possible to place it too close to the airfoil. This effect is easier to understand in Section 3.4, where the velocity spectra are studied in detail. Regarding the stream turbulence intensity contour map (Fig. 5), the -2.5° is the angle that shows a largest turbulence intensity, around 11%. The contour map has been saturated at 6% to provide a clear view of the turbulence intensity variations. On the other hand, the 2.5° has the lowest turbulence levels (4%), as shown in Fig. 5. These results are in good agreement with the observations found for the Reynolds stress tensor, which are discussed in the next section.

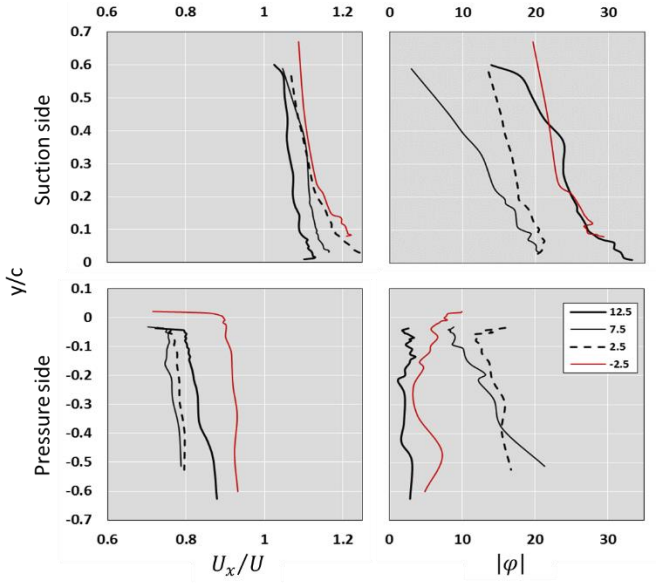

Fig. 6. Longitudinal velocity component measurements and angle between the total velocity and the longitudinal velocity component of the flow in the airfoil.

3.2 Reynolds stress tensor.

In general, there are six independent components of the Reynolds stress tensor: $\overline{u'^2}$, $\overline{v'^2}$, $\overline{w'^2}$, $\overline{u'v'}$, $\overline{u'w'}$ and $\overline{v'w'}$, where *u'*, *v'* and *w'* represent the fluctuation velocity components in the three spatial directions. However, because of the nature of the velocity field, sometimes one or more of these components are zero. In this case, the Reynolds stress $\overline{u'w'}$ and $\overline{v'w'}$are negligible throughout the flow is statistically 2-D on x-y plane in the z-direction.

A. Wake

Figure 7 depicts, the Reynolds stress components. The data has been made dimensionless with the squared free-stream velocity. The streamwise fluctuation (*u'*) distributions display a characteristic two-peaked profile in the instability zone, which is clearer for the positive incidence angles. Tulapurkara et al. (1994) and Weygandt and Mehta (1995) showed the same double peak in the wake for a tripped boundary layer airfoil and Farsimadan and Dehghan (2010) for an untripped boundary layer one, as in this study. The results from the different authors indicated that a positive increase in the angle of attack makes the two-peaked behavior more visible. As the angle is modified, the boundary layer in the upper surface is thicker, resulting in more highlighted double peaks, as can be seen for α=12.5° in Fig. 7.

As far as normal fluctuations (*v'*) are concerned, a single peak is shown in Fig. 7 for all the angles. The magnitude of the normal velocity fluctuations is higher than for the streamwise fluctuations, becoming the most important flow component. Regarding the $\overline{u'v'}$ graph from Fig. 7, the more relevant characteristic is the sign change at the wake center, which coincides with the minimum velocity location. This change of sign is clearer for the positive angles rather than for the negative one, showing a positive peak on the pressure side and a negative peak on the suction side in their velocity profiles. In addition, the pressure side peak is smaller than the suction side one, increasing this difference with the angle of attack. It should be pointed out that the wake asymmetry observed in the velocity profiles is clearly depicted in Fig. 7, especially in the $\overline{u'v'}$ graph, increasing with positive angles.

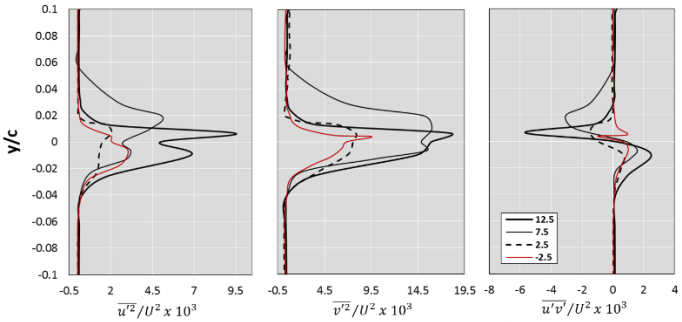

Fig. 7. Reynolds stress components in the wake (L1).

Normally, the width wake is estimated through the velocity distributions as well as the wake depth. However, in this paper, concerning to the width wake, the Reynolds stress components are used instead the direct lecture from velocity distributions. These components show the instability zone with great clarity and help to identify the wake width with more accuracy than the classical procedure (Fig. 8 Right). The wake width, estimated using the Reynolds stress components where the white dots enclose the instability area, and the wake depth are depicted in Fig. 8. As expected, both increase with the angle of incidence and are very similar for the intermediate angles, concluding that the angle 12.5° presents the greatest wake dimensions.

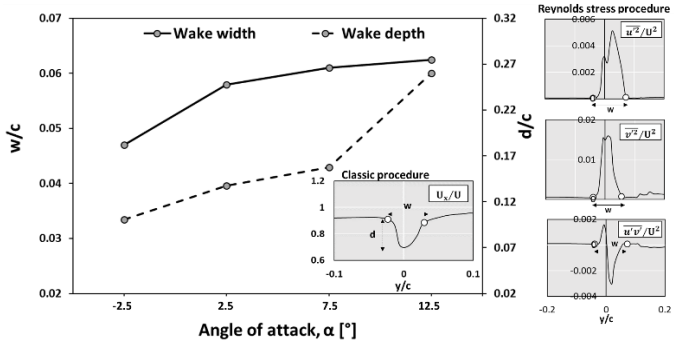

Fig. 8. Wake dimensions and Reynolds stress components use to estimate the width and depth wake.

B. Airfoil

At this localization (L2), the most remarkable result is the increase of the velocity fluctuations inside the boundary layer as a consequence of the developed shear stresses. For positive incidence angles, the flow follows the airfoil shape at the suction side due to its smooth curvature. This is the reason why it is very hard to obtain enough

measurements on this side of the airfoil. Nevertheless, the increase in the incidence angle allows to capture part of the boundary layer. On the pressure side, the high curvature of the airfoil at the probe location widens the boundary layer, enabling the possibility of obtaining more data. For the negative angle, the behaviors of the pressure and suction sides interchange, and so does the behavior of the flow. The suction side boundary layer becomes even more adhered to the surface and it is impossible to measure inside it. On the pressure side, the widening of the boundary layer due to the high curvature allows to perform more measurements, as for the positive angles.

Additionally, as well as in the wake, the normal velocity fluctuations were found to be higher than the streamwise ones. The turbulence, as expected, is lower than in the wake region, with lower values of the Reynolds stresses concentrated inside the boundary layers.

As the behavior in this position is very similar to the wake, the total production term of the turbulence kinetic energy budget ($P_{k,\,total}$) is calculated instead of depicting the Reynolds stress components to visualize the effect of the airfoil geometry in the turbulence management. For the case of simple shear flow, this term represents the generation of turbulence energy by the interaction between the Reynolds shear stress ($-\overline{u'v'}$) and the mean flow shear strain ($\partial U/\partial y$), i.e., the transfer of energy from the mean flow to the turbulence field. However, there are some limitations for this approach when the strain conditions are modified, as studied by Leschziner (2015). As a solution for partially addressing these limitations, a number of corrections are proposed. Some complex flows need to combine shear with some corrections such as for curvature, swirl, rotation or buoyancy effects to achieve more accurate results. In this case, the high curvature of the airfoil implies the combination of the production term with the curvature correction. According with Leschziner (2015), turbulence energy, with the curvature included, is generated at the rate:

$$P_{k,total} = \underbrace{\overline{-u'_\theta v'}\frac{\partial U_\theta}{\partial y}}_{shear} + \underbrace{\overline{u'_\theta v'}\frac{U_\theta}{R_c}}_{curvature} \qquad (2)$$

Where v' is the mean fluctuation of the normal velocity component of the flow, u_Θ' is the mean fluctuation of the tangential velocity component of the flow in polar coordinates, U_Θ is the mean tangential velocity in polar coordinates and R_c is the radius of curvature of the airfoil.

Figure 9 shows on its left side the total production term including the curvature correction. For the sake of clarity, a zoom in the airfoil surface is performed on the right side of Fig. 9 for the angle 12.5°. In addition, the different contributions of the equation (2) to the total production, corresponding to the curvature and the shear term, are depicted. It can be appreciated that shear is the primary source of instabilities, so Pk_{shear} and Pk_{total} present similar values and therefore Fig. 9 (left) describes both variables. Firstly, the coexistence of mean strain and turbulent fluctuations ($P_{k,\,shear}$) gives rise to a continuous generation of turbulence that compensates for viscous dissipation. Pk_{shear} represents the rate at which kinetic energy is lost by the mean flow and gained by the turbulence fluctuations.

In Fig. 9, it can be seen for both airfoil sides, in the closest region to the airfoil surface, the Pk_{total} presents negative values. These negative values in the instability zones are translated in a generation of turbulent energy which implies high friction and therefore a higher resistance to the mean flow. In this zone, the turbulent field gain energy and the mean flow lost it. The negative angle pressure side and the suction side for the highest positive angle are the most characteristic graphs, where Pk_{total} reach the most negative values. These two zones correspond with the most instability zones of all the cases represented. On one hand, on the pressure side of the -2.5 angle the boundary layer is broaden due to the high curvature of the airfoil in this region, while on the 12.5 angle suction side the boundary layer expansion is due to the beginning of the flow separation to increase the angle of attack. For this reason, the shear stress caused by the flow is of great importance for friction drag calculations, providing a clear idea of the flow resistance.

The second parameter to consider is the effect of the curvature on the total production term ($P_{k,\,curvature}$). This term contributes to stabilize the flow on both airfoil sides. Both suction and pressure sides, the curvature, due to be opposite sign to the shear, favors to reduce the turbulence, depressing the turbulence and benefiting the increment of the total energy gained by the mean flow and consequently reduces the airfoil resistance to the flow. This positive effect on both sides is probably owing to curvature, which helps to keep the flow adhered to the surface.

3.3 Degree of anisotropy

The degree of anisotropy (DA), as defined by Porreca et al. (2005), is a flow indicator which compares fluctuating velocity components in the two directions, so departures from isotropy associated to turbulence can be quantified. As the Reynolds stress shown before, as much at the wake as on the airfoil, the transversal fluctuation is notably higher than the longitudinal one, so the degree of anisotropy is calculated according to:

$$DA = \frac{\left(\overline{v'^2} - \overline{u'^2}\right)}{\overline{v'^2}} \qquad (3)$$

where the over bar denotes the time-averaging value, and the u'^2 and v'^2 represent the squared random fluctuations in the longitudinal and transversal directions, respectively.

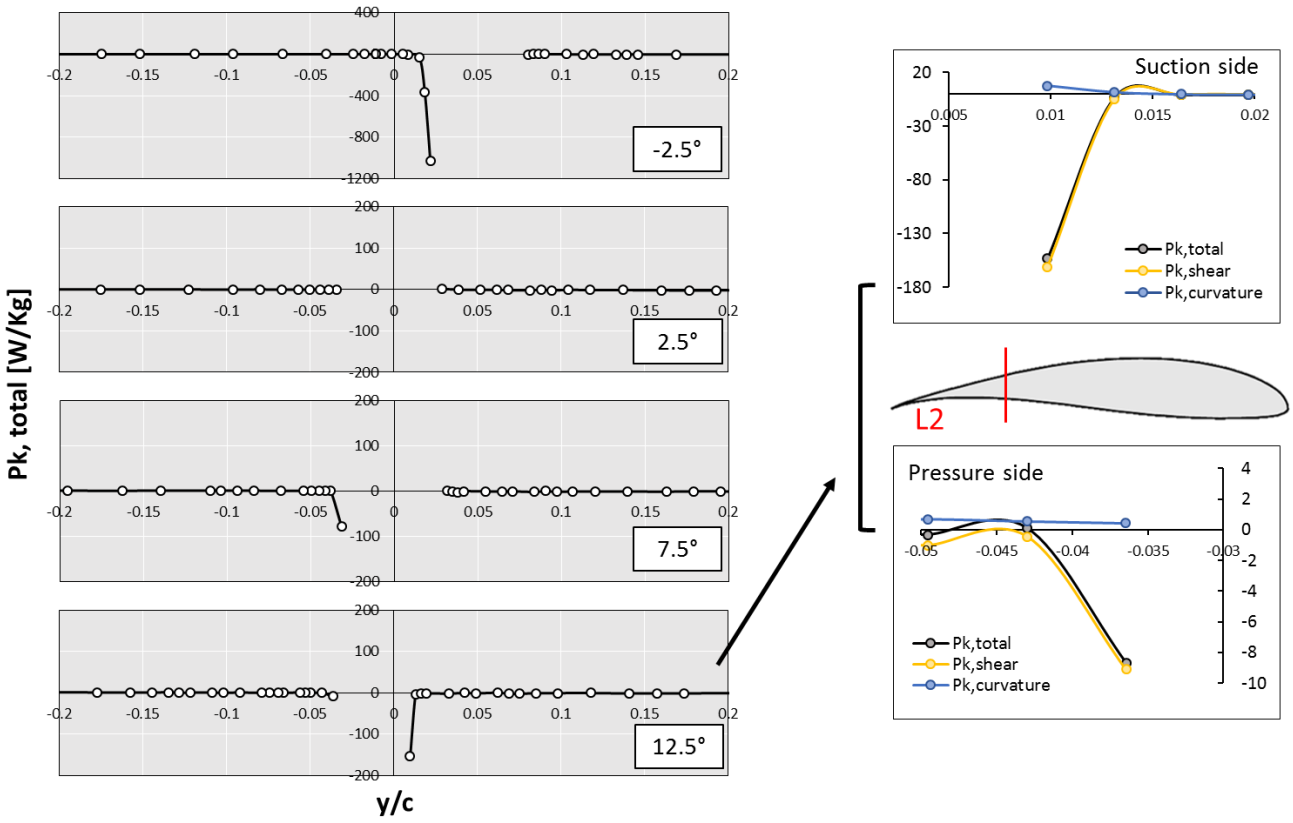

Fig. 9. Total turbulent energy production term with the curvature contribution included (Left). Zoom of the breakdown of the total turbulent energy production in the corresponding curvature and shear terms for the angle 12.5°, corresponding the X-axis with Y-coordinate values (Right).

If the turbulent fluctuations are completely isotropic, i.e., if they do not have any directional preference, then the off-diagonal components of $\overline{u'v'}$ vanish, and the normal stresses become equal (Kundu, et al., 2016). Hence, when DA tends to unity, it is satisfied that $\overline{v'^2} \gg \overline{u'^2}$ and the flow is completely anisotropic having a transversal directional preference. On the other hand, if DA tends to zero, it means that $\overline{v'^2} \sim \overline{u'^2}$, and the flow is isotropic.

A. Wake

In this case, as can be seen in Fig. 10 (Left), there is a clear anisotropy in the outlying area of the sweep. In most part of the flow, the transversal fluctuations are as high as 20-40 times the longitudinal ones. The distinctive feature of the Fig. 10 is a characteristic double peak with a "W" shape, where the local minimum between the two peaks corresponds with the point where the velocity profile reaches its minimum. This point also agrees with remarkable points at the Reynolds stress components graphs, such as the inflection point of the $\overline{u'v'}$ component or the minimum local of the double peak of the $\overline{u'^2}$ component.

The double peak shows the most isotropic points in the distribution, forming an anisotropic area between them. In Fig. 10, the white dots drawn at the graph represent the end of the transition zone introduced in the last section. The degree of anisotropy is a useful parameter that provides reliable and clear information about the transition zone. This transition zone can be easily seen in the graphs, which supports the Power Spectral Density graphs. When the flow approaches to the wake, the instabilities start to be produced in a zone near to it where all the components of the flow tend to isotropy and thus are similar. In addition, this instabilities are lower than those produced inside the wake. This feature can be seen in the Reynolds stress components, where only the high instabilities produced in the wake are shown.

Comparing the anisotropy and the Reynolds stress values, it is clearly seen that the isotropic points present the lowest differences between the Reynolds stress components, with any of the flow components outlined over the rest.

B. Airfoil

As can be seen in Fig. 10 (Right), the behavior of the degree of anisotropy over the airfoil is very similar to its behavior at the wake. The anisotropic region matches the farthest zone of the sweep. The transversal fluctuations on the bulk of the flow are as high as 10-25 times the longitudinal fluctuations. As the flow approaches the airfoil, the anisotropy decreases, reaching a point of maximum isotropy and then returning again to anisotropy values. This anisotropic behavior inside the unsteady region is due to the presence of shear, the most frequent type of forcing. When shear stresses appear, the eddies are elongated and the intensity of the fluctuations can be very different in different directions. At this airfoil position, the most isotropic point agrees with the beginning of the boundary layer and from this point, inside the boundary layer, the flow tends to anisotropy. As in the wake, this point coincides with the locations with the smallest difference between transversal and longitudinal Reynolds stress components, i.e., the point where the boundary layer starts. It can be seen that for the negative incidence angle, where the suction side was impossible to be measured, the values do not reach a minimum and thus it is not possible to know where the boundary layer starts.

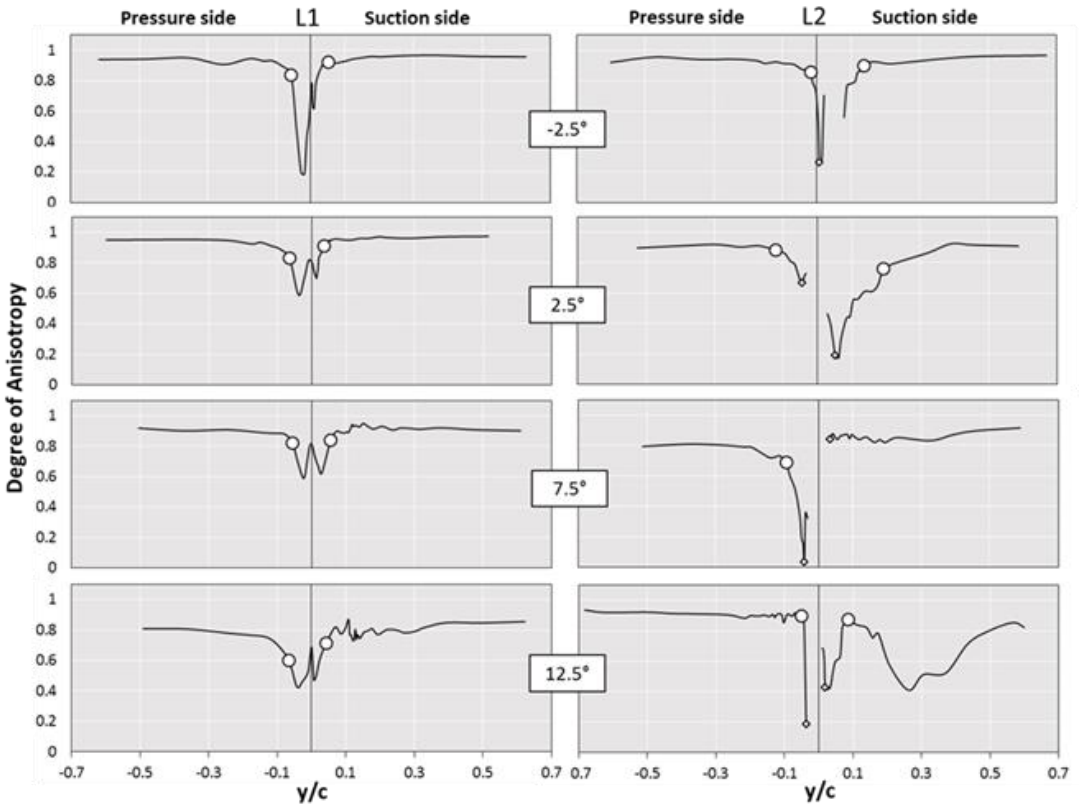

Fig. 10. Degree of anisotropy at L1 (Wake) and L2 (Airfoil) positions. White dots represent the end of the transition zone.

On the other hand, on the pressure side for the 12.5 angle, although the anisotropy values do not increase after the maximum isotropic point, it is known that this point belongs to the boundary layer due to the results from the Reynolds stress components graphs, where it appears as a high instability point. Additionally, the existence of a single measure point in this localization agrees with the theory that on this pressure side for this angle the boundary layer is the thinnest. Finally, for the suction side at 7.5° angle, all the values are anisotropic and it is neither possible to estimate the boundary layer nor the transition zone. For this reason, a detailed study of different parameters related with turbulence is necessary as only a combination of them allows the complete understanding of the turbulence structure.

3.4 Velocity Spectra

The power spectral density (PSD) of the normal velocity measurements is analyzed in order to know how the power of a signal in the time domain is distributed over the different frequencies. The PSD function is a very useful tool to identify oscillatory signals and at which frequency ranges variations are stronger. Several authors (Cao, 2010; Huang & Lee, 2000; Cambell, 1957), determined the vortex shedding frequency behind an airfoil using the power spectral density analysis. In the following pictures, both frequency and power axis are plotted in a logarithmic scale and only three angles are depicted to improve the resolution of the important features.

A. Wake

The PSD's based on the normal velocities at all the sweep localizations were estimated. Firstly, modifications in the power spectrum tendency throughout the sweep are perfectly seen in Fig. 11. These changes in the shape and the slope of the PSD are colored in the two-colored graphic. The instabilities produced inside the wake region are depicted by red and agree with the wake width estimated in the previous section, as well as with the zone of velocity deficit, as shown in Fig. 11 (below the PSD). For this reason, it can be concluded that the total instability region is formed by the own wake and a lower unsteady contiguous zone, named in this paper as the "transition zone". This transition zone is a zone outside the wake between it and the free stream zone, where the values are still affected by the wake instabilities. The zone appears colored in grey in the PSDs graphs. The degree of anisotropy calculated in the previous section also supports this hypothesis. However, the transition zone does not appear in the Reynolds stress components obtained in Section 3.2. It can be concluded thus that the instabilities in this transition zone are much lower than in the own wake. In addition, there is no evidence of any frequency related with vortex shedding due to the absence of highlighted peaks relative to the background energy levels in the PSD, i.e. of any periodic phenomenon appearing in the flow. As a consequence, no noise generated by vortex shedding is expected to be found when performing further aeroacoustic analyses.

B. Airfoil

Focusing on the airfoil position (L2), the power spectral distributions in Fig. 11 show the same general results that for the wake. The shape of the PSD is modified when the measurements are made inside the boundary layer. As for the wake, two colors are also used to difference the zones: red to highlight the boundary layer and grey to illustrate the transition zone. As for the wake, it is assumed that the transition zone instabilities are lower than the boundary layer instabilities due to the lack of transition instabilities in the Reynolds stress graphs. For this case, on the suction side, the transition zone is not colored because it is very difficult to visualize the extent of this

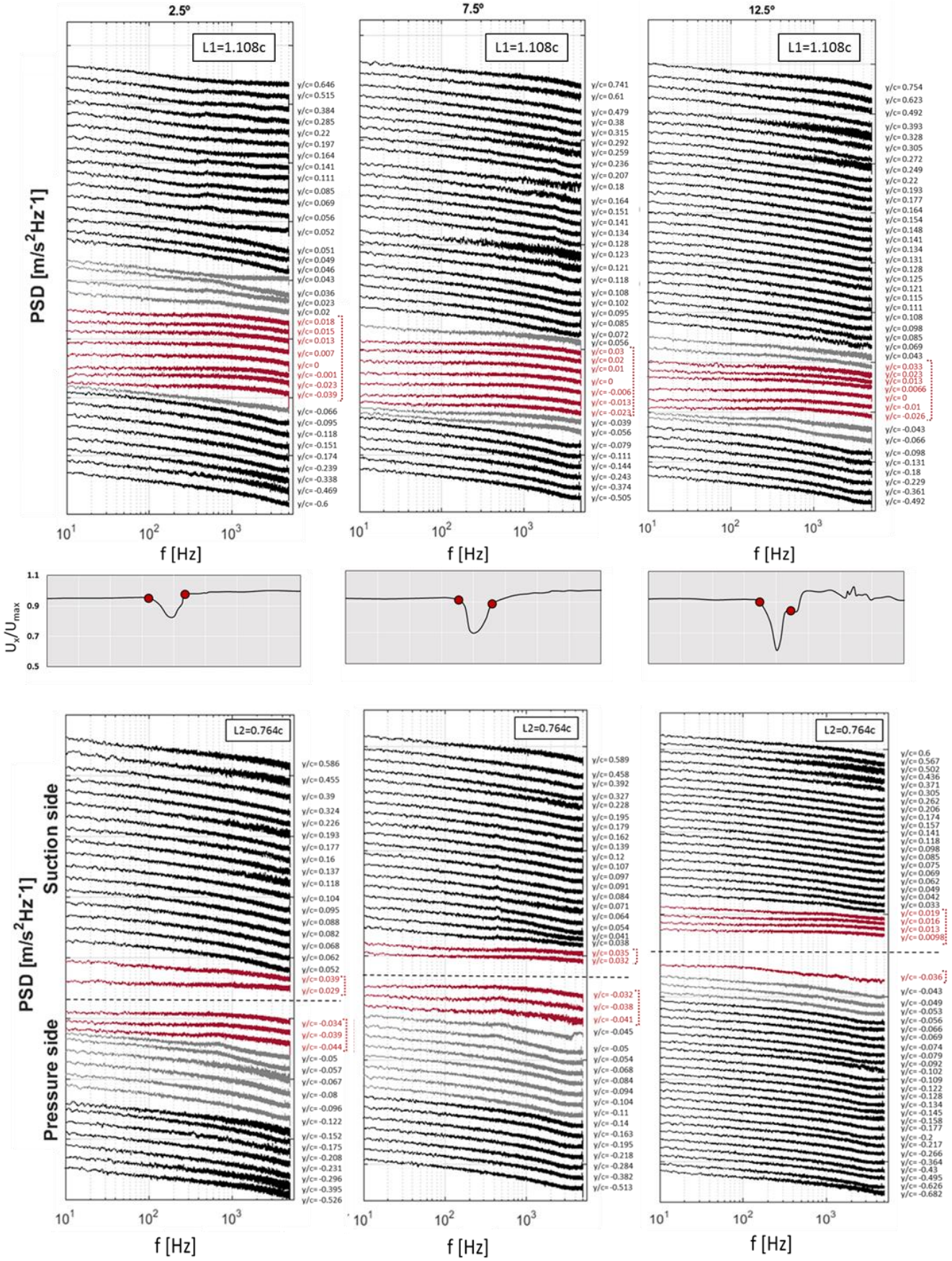

Fig. 11. Power spectral density of the normal velocity at the L1 (Wake) and L2 (Airfoil) position for 2.5°, 7.5° and 12.5° angles. Longitudinal velocity distributions (middle). Red dots represent the localizations where the wake finishes.

zone basing the observation on the PSD results. However, it is possible to detect it in the previous section graphs, where the degree of anisotropy is estimated. Additionally, the main disadvantage of the hot-wire technique are appreciated in this figure. The fragility of the wire does not allow to measure very close to the surface airfoil. Consequently, few measures can be performed inside a thin boundary layer. Even so, with a simple sight at the picture, it is possible to know that the boundary layer on the suction side is smaller than on the pressure side. This behavior can be explained by the higher airfoil curvature on the pressure side, which prevents the flow from maintaining a thin boundary layer along the pressure surface. As a consequence, a boundary layer widening effect appears at the highest curvature points of the airfoil. For the sake of clarity, a 2D-RANS CFD was simulated. A k-omega turbulence model and a $1.1x10^5$ structured mesh were used for the same flow conditions as for the experimental tests. Figure 12 shows the results for the velocity magnitude, where the boundary layer is clearly depicted, corroborating the above-mentioned behavior for the different angles: the suction side boundary layer is extremely thin, while the pressure side boundary layer is easier to measure, except for the 12.5° angle, for which these behaviors interchange. For this angle, it was only possible to obtain one experimental value inside the pressure side boundary layer.

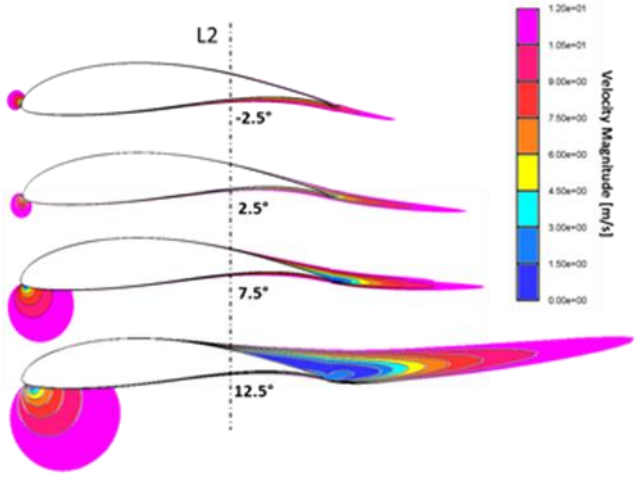

Fig. 12. Contours of velocity magnitude obtained by CFD simulation.

3.5 Integral Length Scale

One of the most significant turbulence parameters in this contexts is the Integral Length Scale (ILS). This indicator assigns a spatial dimension to the turbulence structure, often identified as the average eddy size. The autocorrelation analysis of random fluctuations was used to estimate Integral Length Scale, which was determined by:

$$ILS = \overline{U} \int_0^{\infty} \frac{\overline{u'(t) + u'(t+\tau)}}{\overline{u'^2}} d\tau \qquad (4)$$

Where the parameter integrated is the AutoCorrelation Function (ACF), the over bar denotes the time-averaging value and τ is the time lag that is used to construct the ACF.

This formulation assumes that the average eddy size lies through the correlation of two velocity signals. To estimate the Integral Length Scale in Eq. (4), it is necessary to evaluate the correlation coefficient of the velocity fluctuations (in time), because the area under the correlation gives the value of the Integral Scale. Some authors (Fernández Oro, et al., 2008; Fernández Oro, et al., 2007) used the first zero as the main criterion to calculate the area under the ACF, while depending of the characteristics of the database, Tropea et al. (2007) suggests alternative methods. In our measurements, the first minimum criterion is chosen to estimate the extension for the Integral Length Scale.

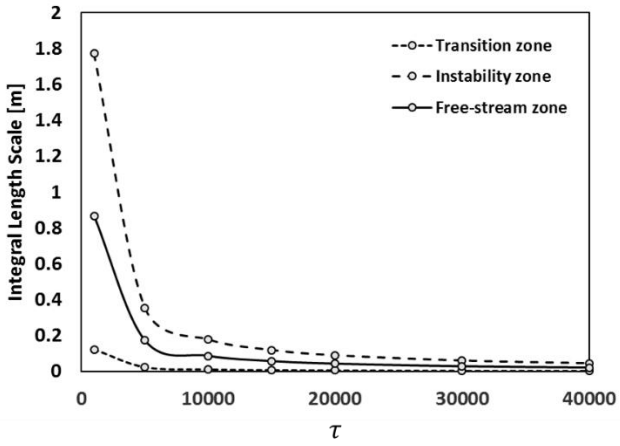

It is evident for the high degree of disparity and the inherent uncertainty to define an exact value of the Integral Length Scale, that only an approximate order of magnitude and an overall trend can be given regarding this parameter. Consequently, in this section only the wake results are presented.

In Fig. 13 it can be distinguished three areas: instability, transition and free-stream zone, according to the previous results. The instability area existent in the wake is represented by a light grey shaded area, where the smallest Integral Length Scales are localized with values very close to zero. The darker grey area represents the transition zone. In this region the ILS increases in comparison to the instability zone and it is characterized by presenting greater variations in eddies size. In contrast, these variations do not appear in the free-stream zone, where the size is more uniform. In general, both localizations present an increase of the Integral Length Scale with the angle of attack and therefore also increasing eddies size. The maximum value of the ILS is around 0.5 m, concluding that the eddy sizes vary inside the instability zone until a minimal size, when the eddies become dissipated in the free-stream flow.

4. Conclusions

A detailed experimental characterization of the turbulence structure around an asymmetric high-lift airfoil for different incidence angles has been carried out. The velocity field measurements, using hot-wire technique, allow the study of different turbulence parameters such as turbulence intensity, degree of anisotropy or integral length scale among others. Additionally, the velocity spectra are analyzed to identify the existence of periodic phenomena in the flow. Relevant flow information is obtained when the frequency and anisotropy analyses are combined.

On the whole, the findings have shown good agreement with the results of previous works, besides adding information to the understanding of the turbulence structure around a FX 63-137 airfoil. The results revealed the behavior of the boundary layer and the wake depending on the incidence angle.

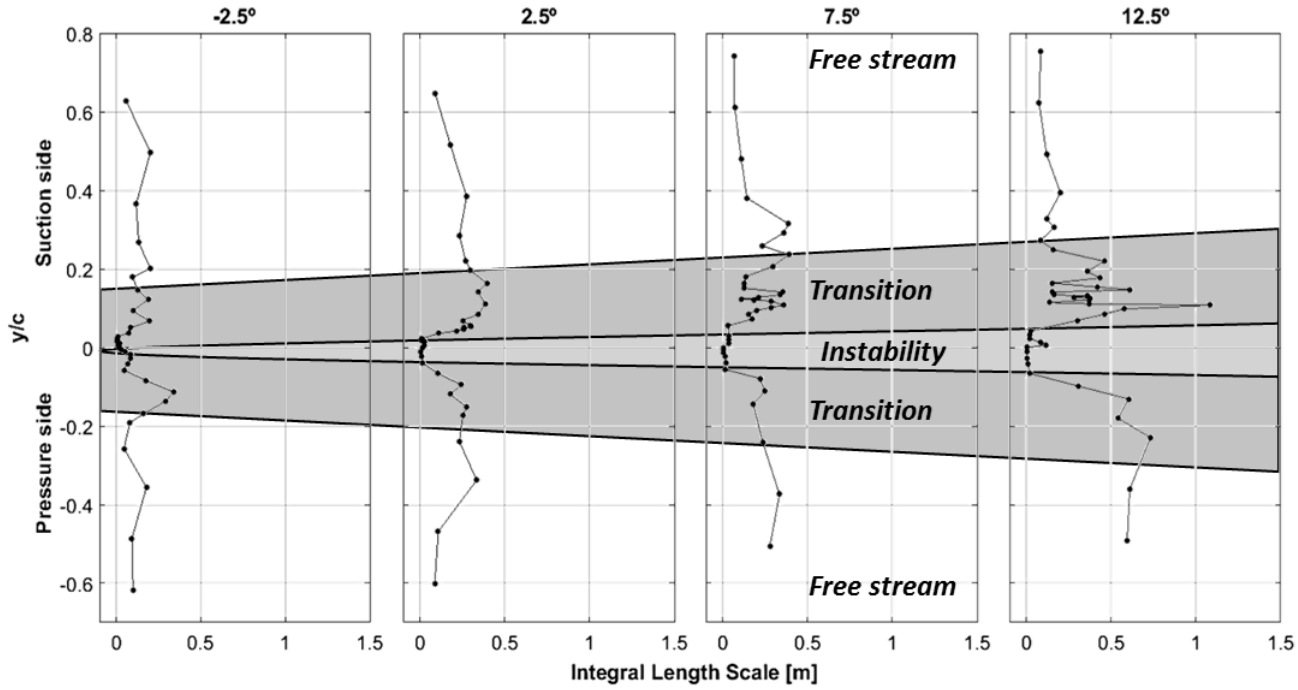

Fig. 13. Integral Length Scale for L1 (Wake) localizations.

The airfoil geometry and the angle of attack are the main causes of the asymmetric wake. The increase of the asymmetric shape of the wake with the incidence angle was analyzed through the velocity measurements and the Reynolds stress tensor. The Reynolds stress components were used to estimate the wake width accurately and visibly, disclosing a width increment with the incidence angle. As a result, the 12.5° angle presents the greatest instability zone and the highest level of turbulence on the suction side of the wake. However, the -2.5° angle shows a high level of turbulence on the pressure side due to the asymmetry of the airfoil and the direction of the incident flow. The detailed study of the coupling between velocity spectra and anisotropic behavior discloses three different regions: an instability zone, a transition zone where the flow is still affected by the wake instabilities and a more uniform area called free-stream zone. The transition instabilities present two characteristic features: they are much lower than the instabilities at the wake and tend to isotropy.

Additionally, the velocity spectra support the wake analysis, besides not presenting any relevant peak related with vortex shedding. This fact removes vortex shedding as one of the possible aerodynamic noise generation mechanisms for the FX 63-137 airfoil. However, this hypothesis must be checked by means of further aeroacoustic analysis.

On the airfoil localization, the boundary layer is well estimated through the Reynolds stress components for all the angles. With an increase in the angle of attack, the boundary layer width decreases on the pressure side, while it increases on the suction side. On the pressure side, the flow is attached to the airfoil surface; however, the high curvature region of the airfoil causes a widening in the boundary layer. For this reason, the boundary layer is easier identified on this side. On the contrary, on the suction side, a smoother curvature is present in the airfoil geometry so the flow is highly adhered to the surface, originating a thin boundary layer which increases with the incidence angle. For the negative angle, the pressure side and the suction side interchange. Consequently, the boundary layer is so thin on the suction side that it is not possible to measure inside it for this angle. For all the angles, turbulence energy is produced on the suction side and reduced on the pressure side. On both cases, the curvature of the airfoil helps to stabilize the flow. The shear term is the main source of resistance to the flow and a basic parameter to estimate and understand the friction drag, which is a contributor of the total drag. As for the wake, the combination of the PSD and the degree of anisotropy analyses show a similar transition zone between the free-stream and the boundary layer with analogous features. However, this localization differs with the wake in the fact that the most isotropic point agrees with the beginning of the unsteady zone, in this case the beginning of the boundary layer.

At both localizations, the analysis of all the turbulence parameters provides us a useful tool to characterize the flow around the airfoil. In general, the normal velocity component of the flow is more important than the longitudinal ones. Complementarily, in the free-stream zone the flow is anisotropic, modifying its tendency towards isotropy in the transition zone and then returning to the anisotropy condition inside the unsteady region, where the average turbulent eddies are smaller.

To summarize, only a combination of different turbulence-related parameters allows a complete understanding of the turbulence structure. The results obtained in this work contribute to explain the turbulence characteristics and supplement the information about the flow conditions around an asymmetric high-lift airfoil, offering the opportunity to identify noise generation mechanisms for its analysis in further stages. Moreover, the turbulence data management carried out in this paper represents another set of means for future friction drag reduction studies that will improve wind turbine performances.

Acknowledgements

This work has been supported by Project “Caracterización y predicción de la generación aerodinámica de ruido en perfiles de turbinas eólicas”, DPI2011-25419 by the Spanish Ministry of

Economy and Competitiveness and “Severo Ochoa” predoctoral research grant provided by the Principality of Asturias, Spain

5. Referencias

Blanco, E., Ballesteros, R. & Santolaria, C., 1998. Angular range and uncertainty analysis of non-orthogonal crossed hot wire probes. *Journal of Fluids Engineering*, Volumen 120, pp. 90-94.

Brooks, T. & Marcolini, M., 1986. Airfoil tip vortex formation noise. *AIAA Journal*, 24(2), pp. 246-252.

Cambell, G., 1957. *Turbulence in the wake of a thin airfoil at low speeds*, Washington DC, USA: Technical memorandum 1427, National Advisory Comittee for Aeronautics.

Camp, T. & Shin, H., 1995. Turbulence intensity and length scale measurements in multistage compressors. *ASME Journal Turbomachinery*, Volumen 117, pp. 38-46.

Cao, N., 2010. Effects of turbulence intensity and integral length scale on an asymmetric airfoil at low Reynolds numbers. *PhD dissertation.*

Farsimadan, E. & Dehghan, M., 2010. An experimental study of the turbulence quantities in the boundary layer and near wake of an airfoil placed at upstream of a 90º bend. *Experiments in Thermal and Fluid Science*, Volumen 34, pp. 979-999.

Fernández Oro, J., Argüelles Díaz, K., Santolaria Morros, C. & Blanco Marigorta, E., 2007a. Unsteady flow and wake transport in a low speed axial fan with inlet guide vanes. *Journal of Fluid engineering*, Volumen 129, pp. 1015-1029.

Fernández Oro, J., Argüelles Díaz, K., Santolaria Morros, C. & Blanco Marigorta, E., 2007. On the structure of turbulence in a low-speed axial fan with inlet guide vanes. *Experimental Thermal Fluid Science*, 32(1), pp. 316-331.

Fernández Oro, J. y otros, 2008. Turbulence and secondary flows in an axial flow fan with variable pitch blades. *ASME Journal of Fluids Engineering*, Volumen 130, pp. 1-11.

Hah, C. & Lakshminarayana, B., 1982. Measurement and prediction of mean velocity and turbulence structure in the near wake of an airfoil. *Journal of Fluid Mechanics*, Volumen 115, pp. 251-282.

Huang, R. & Lee, H., 2000. Turbulence effect on frequency characteristics of unsteady motions in wake of wing. *AIAA Journal*, 38(1), pp. 87-94.

Kundu, P., Cohen, I. & Dowling, D., 2016. *Fluid Mechanics.* 6th ed. London: Academic Press.

Kunze, C., 2004. Acoustic and velocity measurements in the flow past and airfoil trailing edge. *Trabajo fin de Máster.*

Lastra, M. y otros, 2013. Novel design and experimental validation of a contraction nozzel for aerodynamic measurements in a subsonic wind tunnel. *Journal of Wind Engineering and Industrial Aerodynamics*, Volumen 118, pp. 35-43.

Leschziner, M., 2015. *Statisticale turbulence modelling for fluid dynamics-demystified: an introductory text for graduate engineering students.* London: Imperial College Press.

Liu, X., 2001. *A study of wake development and structure in constant pressure gradients*, Notre Dame: PhD dissertation, University of Notre Dame.

Moldano, V., Castillo, L., Thorman, A. & Meneveau, C., 2015. The role of the free stream turbulence with large integral scale on the aerodynamic performance of an experimental low Reynolds number S809 wind turbine blade. *Journal of wind engineering and industrial aerodynamics*, Volumen 142, p. 246.

Nakano, T., Fujisawa, N. & Lee, S., 2006. Measurement of tonal noise characteristics and periodic flow structure around NACA0018 airfoil. *Experiments in Fluids*, Volumen 40, pp. 482-490.

Porreca, L., Hollestein, M., Kalfas, A. & Abahari, R., 2005. *Turbulence measurements and analysis in a multistage axial turbine.* Munich, s.n.

Selig, M. & McGranahan, B., 2004. Wind Tunnel Aerodynamic Tests of Six Airfoils for Use on Small Wind Turbines. *Journal of Solar Energy Engineering*, Volumen 126, pp. 986-1001.

Tropea, C., Yarin, A. & Foss, J., 2007. *Handbook of Experimental Fluid Mechanics.* s.l.:Springer.

Tulapurkara, E., Ramjee, V. & Jacob, G., 1994. Development of wake in presence of both curvature and pressure gradient. *Boundary layer and Free Shear Flows, ASME*, Volumen 184, pp. 195-202.

Velarde-Suarez, S., Ballesteros-Tajadura, R., Santolaria-Morros, C. & Blanco-Marigorta, E., 2002. Total unsteadiness downstream of an axial flow fan with variable pitch blades. *ASME Journal of Fluids Engineering*, Volumen 124, pp. 280-283.

Weygandt, J. & Mehta, R., 1995. Three dimensional structure of straigth and curved plane wakes. *Journal of Fluid Mechanics*, Volumen 282, pp. 279-311.

Yarusevych, S., Sullivan, P. & Kawall, J., 2004. *Investigacion of airfoil boundary layer and wake development at low Reynolds numbers.* Portland, Oregon, s.n.

ç